JOTCS A
Journal of the Turkish Chemical Society Section: A Chemistry
TURKISH CHEMICAL SOCIETY

Synthesis of Imino Stabilized Iron Oxide Nanosensor for Selective Detection of Lead Ions

Erum Hasan[1], Syed Nawazish Ali[1]*, Ambreen Zia[1], Sabira Begum[2], Salman Tariq Khan[3], and Syeda Farah Bukhari[1]

[1]University of Karachi, Department of Chemistry, 75270, Karachi, Pakistan.
[2]University of Karachi, Department of Chemistry, 75270, Karachi, Pakistan.
[3]Pharmaceutical Research Centre, PCSIR Laboratories Complex, Karachi, 75280, Pakistan.

Abstract: The present work describes the successful preparation of iron oxide nanoparticles (NSB1) stabilized with 4-((2-hydroxybenzylidene)amino)benzoic acid. The characterization has been achieved through ultraviolet visible (UV-Vis), fourier transform infra-red (FTIR) spectroscopy and scanning electron microscopy (SEM) with electron dispersive X-ray elemental analysis (EDX). These magnetic nanoparticles have exhibited significant chemosensing properties in the aqueous media to screen Cr^{3+}, Cd^{2+}, Li^{+}, Co^{2+}, Al^{3+}, Pb^{2+}, Ni^{2+} and Sr^{2+} ions. However, lead (Pb^{2+}) ions have shown the highest selectivity as compared to other metal ions without any interference in the competitive ion study. The detection limit of Pb^{2+} ions was found to be 1.7 µM by this nanosensor. The binding ratio and stoichiometry was found to be 1:1 as measured by Job's plot. The binding strength was also computed through Benesei-Hildebrand equation.

Keywords: Iron oxide nanoparticles, p-aminobenzoic acid, Job's plot, chemosensors, Schiff base, lead ions detection.

Submitted: April 18, 2022. **Accepted:** January 26, 2023.

Cite this: Hasan E, Ali SN, Zia A, Begum S, Khan ST, Bukhari SF. Synthesis of Imino Stabilized Iron Oxide Nanosensor for Selective Detection of Lead Ions. JOTCSA. 2023;(2):277–86.

DOI: https://doi.org/10.18596/jotcsa.1097197.

***Corresponding author. E-mail:** syed.nawazish@gmail.com.

1. INTRODUCTION

Lead ions (Pb^{2+}) are responsible for the contamination of water, food and soil due to their nonbiodegradable nature and accumulation in the environment (1-3). However, trace amount of lead is potent as toxicant (4) and pigment (5). It acts as enzyme inhibitor when it coheres with SH group in proteineous enzyme. Tetramethyl lead , an organic compound of lead, is also exceptionally toxic because it is prone to absorb by the body through mucus membrane and skin (4). Prolong accumulation of Pb^{2+} is lethal for peripheral and central nervous system as it causes numerous life threatening diseases including memory loss, nervous muscles paralysis, hypertension, kidney failure, abnormality in reproductive system, lungs and liver damages (1-4, 6, 7). Lead pollution is also inevitable due to excessive use of lead containing products in our daily life such as coal combustion, gasoline, usage of paint in water supply system and lead acid batteries. Thereby, development of sensitive and reliable methods for lead detection is of great interest across the world.

Normally, lead analysis has been done through various spectrophotometric methods such as liquid phase micro-extraction with atomic absorption spectroscopy (8), inductively coupled plasma mass spectrometry (ICP-MS) (9, 10), dynamic light scattering technique (11, 12), functional nucleic acids (*e.g.* DNA enzymes, aptamers)-based sensors (13), electrochemical (14-16), and optical methods including fluorimetric (17-22), UV-Vis spectrophotometry (23), chemiluminescence (24), visual detection (25), and photonic crystal optrode (26). In present studies, we report ~~the~~ a rapid synthesis of magnetic nanoparticles under mild reaction conditions. These particles are utilized for selective detection of lead ion in the presence of other metal ions resulted in the development of a new chemosensor.

2. EXPERIMENTAL SECTION

2.1. Material

Para aminobenzoic acid (PABA), lead acetate, ferrous sulfate, ferric chloride, and ammonium hydroxide were purchased from Sigma Aldrich.

2.2. Instrumentation

UV-Visible spectra were recorded on Shimadzu UV-240 spectrophotometer in the range of 200-800 nm with 1 cm path length in quartz cell whereas pH was measured by PHS-3B microprocessor pH meter. Infrared spectra have been monitored through FTIR spectrophotometer (Shimadzu IR-Prestige-21) using KBr pellet. EIMS (Mass spectrometry, JEOL JMS600H-1) was performed to confirm the molecular mass of NSB (iminobase). SEM (Scanning electron microscopy, JEOL from Japan, JSM-6380A; Sample coater model#JFC-1500) was used to examine the size and morphological characterization of nanoparticle. Moreover, the elemental composition was obtained by the help of EDX (Energy-dispersive X-ray spectroscopy, Model No: EX-54175IMU, JEOL Japan, the sample was coated up to 300 µA with gold).

2.3. Synthesis of Schiff base

The formation of 4-((2-hydroxybenzylidene)amino)benzoic acid (NSB) was done by the addition of salicylaldehyde (10.0 mmol, 1.06 mL) into a methanolic solution of PABA (10.0 mmol, 1.37 g) in a 100mL round bottom flask for 30 minutes stirring using a magnetic stirrer (Scheme 1). The obtained yellow precipitates of NSB were filtered and washed with methanol (27).

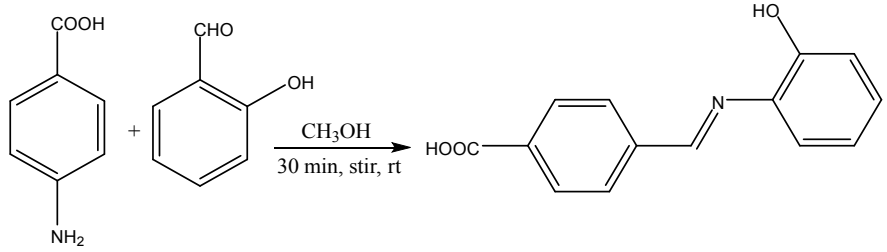

Scheme 1: Synthesis of 4-((2-hydroxybenzylidene)amino)benzoic acid (NSB).

4-((2-hydroxybenzylidene)amino)benzoic acid: Color yellow, Yield: 1.68 g (70%); m.p: 268 °C; FT-IR ($\bar{\upsilon}_{max}$, cm^{-1}): (Stretch, OH) 3426, (sp^2 C–H stretch) 2985, (COO, asymmetric) 1651, (C=C, aromatic) 1593, 1435, (HC=N) 1583, (COO, symmetric) 1377, (C–N) 1288; UV (λ_{max}, nm) 387 π-π* and 321 n-π* transition (azomethine linkage), 245 π-π* transition (aromatic ring); ^{1}H NMR (DMSO-d_6) δ : 11.14 (s, 1H, COOH), 8.26 (d, 2H, J = 8.2 Hz, Ar), 8.18 (d, 2H, J = 8.2 Hz, Ar), 8.16 (s, 1H, HC=N), 7.68 (d, 2H, J = 8.1 Hz, Ar), 7.10 (t, 1H, J = 8.0 Hz, Ar), 6.84 (t, 1H, J = 8.0 Hz, Ar); EIMS (70 eV): m/z 241.

2.4. Preparation of iron oxide nanoparticles (NSB1)

NSB (0.62 g, 4.5 mmol) was dissolved in deionized water (75 mL) at 80 ℃ in a conical flask. An aqueous solution of $FeCl_3.6H_2O$ (1.17 g in 5 mL, 4.3 mmol) was dropwise added into the flask with stirring time of 30 minutes. The aqueous solution of $FeSO_4{\cdot}7H_2O$ (0.94 g in 2 mL, 3.3 mmol) was also added followed by continuous stirring for 30 minutes. Then, NH_4OH (10 mL) was poured and continued to stir for 60 minutes until the brown suspension of NSB1 was obtained (Scheme 2). Washing of nanoparticles was done with deionized water and methanol.

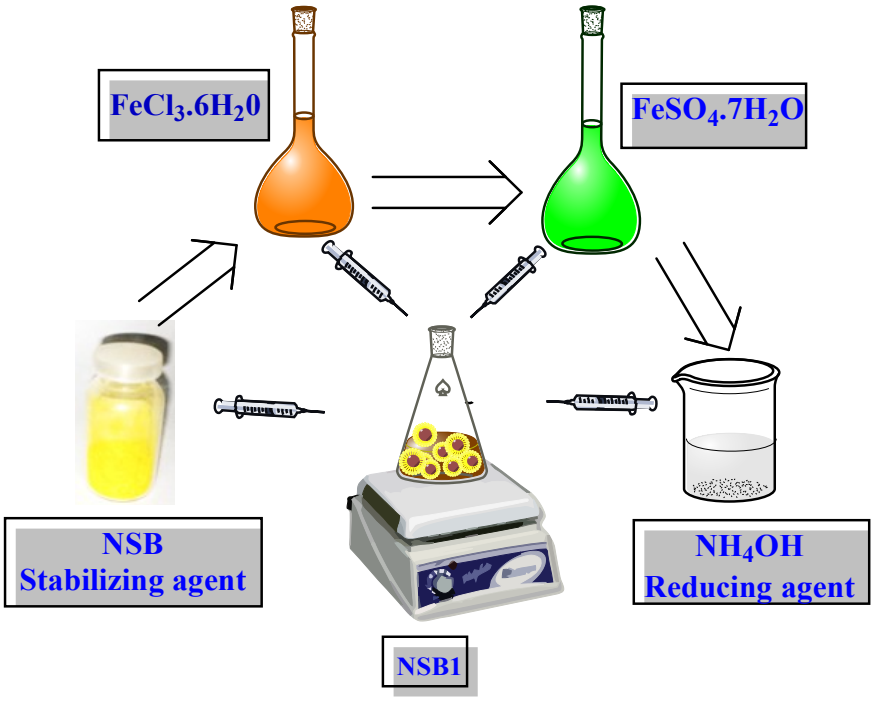

Scheme 2: Synthesis of Iron nanoparticles (NSB1).

3. RESULTS AND DISCUSSION

3.1. NSB and NSB1 comparative FTIR and UV spectra

The FTIR spectrum of NSB and NSB1 were comparatively studied. The absorption band at 3426 cm^{-1} attributes to -OH group whereas the stretching frequencies at 1593 and 1435 cm^{-1} confirms the presence of aromatic C=C functionality. The absorption frequency peak at about 1583 cm^{-1} accredites to HC=N (imine) functional group. The shifting, broadening, and disappearance of certain functional groups show their interaction with nanoparticles for stabilization. The absence of carboxylate stretching frequencies, broadening of aromatic hydrogen peaks (1651 and 1377 cm^{-1}) and weakening of imine group intensity shows the participation of these functionalities (Figure 1). Hence it is anticipated that imine and carbonyl groups work for stabilization of iron nanoparticles.

Ultraviolet visible spectra showed maximum absorbance at 387 and 321 nm due to π-π* and n-π* electronic transition (28) for imine group. On the other hand the absorption maxima at 244 nm was assigned to aromatic acid (Figure 2). The absorption maxima at 260 nm is also in accordance to the reported value of O^{2-}/Fe^{3+} ligand to metal charge transfer transitions to confirm the formation of iron oxide nanoparticles (29). The shifting of absorption maxima also confirmed the involvement of certain functional groups as capping and stabilizing agents.

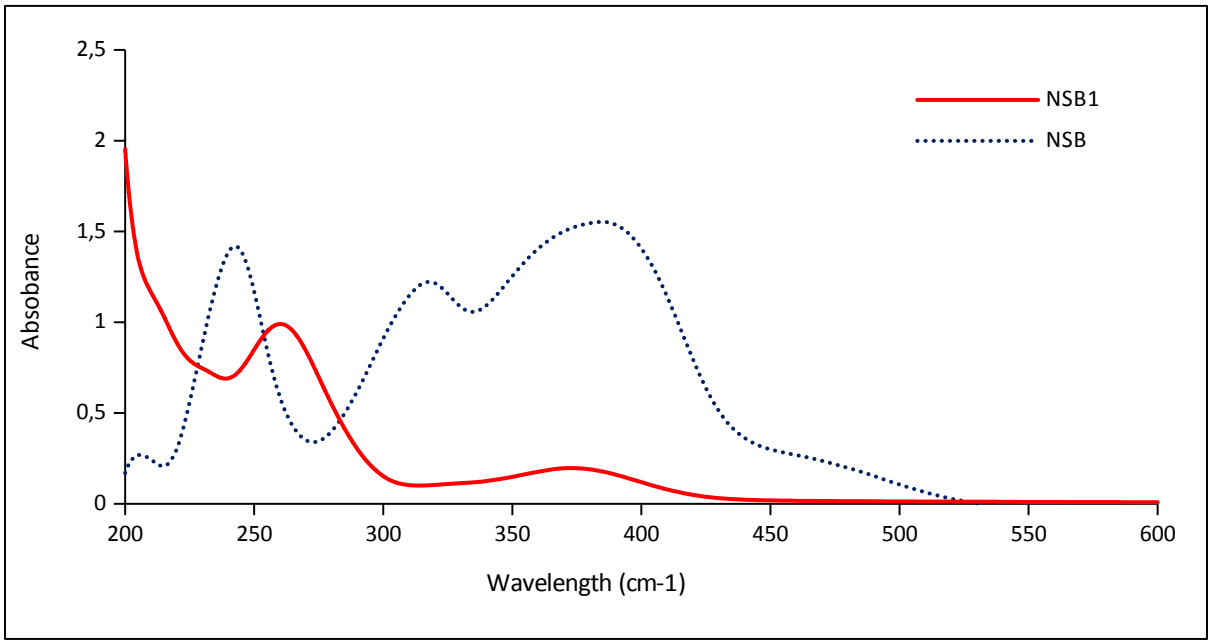

Figure 1: FTIR Spectra of NSB and NSB1.

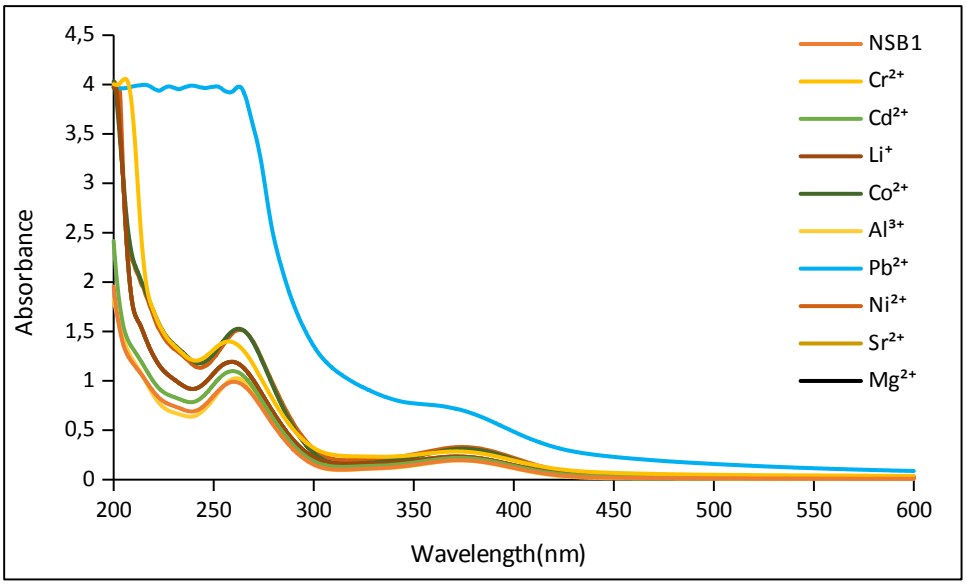

Figure 2: UV-visible spectra of NSB and NSB1.

3.2. SEM and EDX analysis of NSB1

The morphology of iron oxide nanoparticles was analyzed by SEM technique. The obtained results clearly showed the spherically shaped nanoparticles (NSB1) with average size of 87-97 nm (Figure 3).

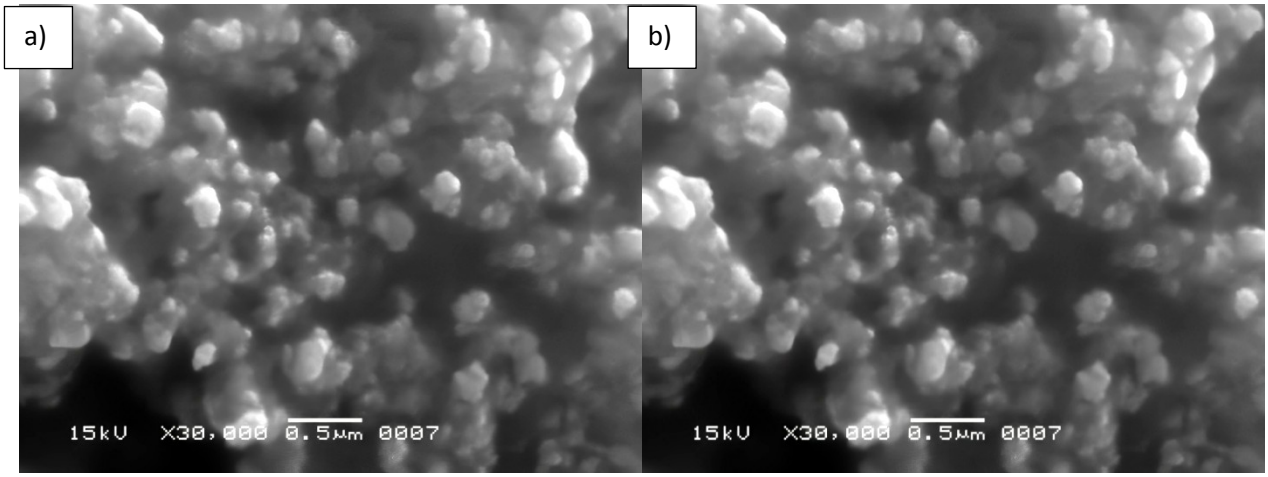

Figure 3: SEM images of NSB1.

EDX analysis also indicates the presence of elements with their mass percentage. However there is slight difference in calculated values due to the presence of other elements. In addition to iron and oxygen, carbon was also appeared due to the interactions of nanoparticles with organic compounds whereas minor quantity of chloride was also observed from other source (Figure 4). Elemental analysis % calculated (observed): Fe 69.94 (74.72), O 30.06 (21.26)

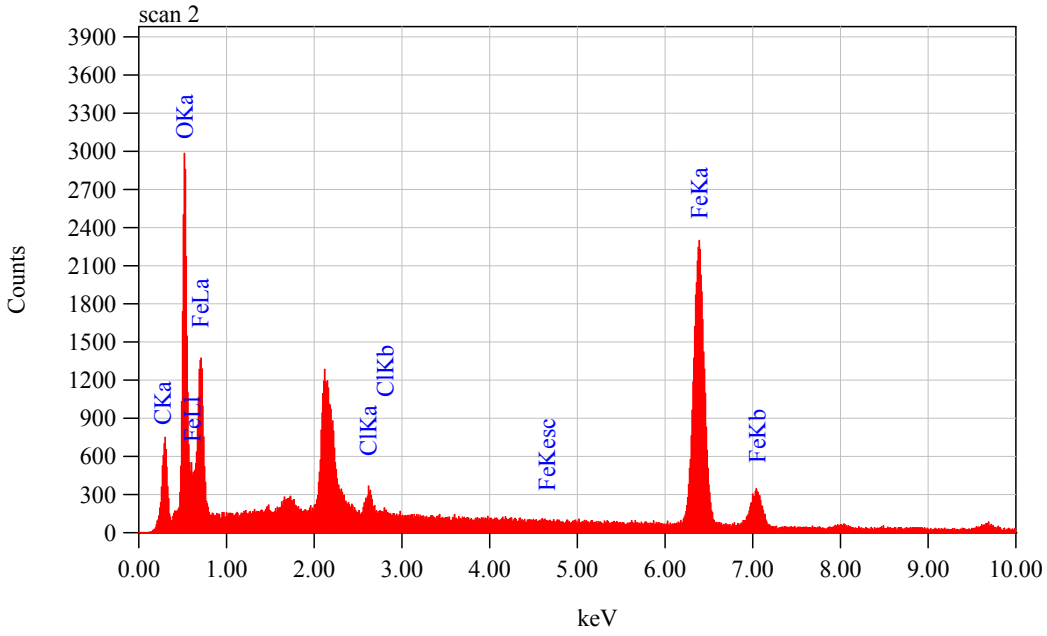

Figure 4: EDX spectrum of chemical elements on iron oxide nanparticles.

3.3. Screening of metal ions

Various metals Cr^{3+}, Cd^{2+}, Li^{+}, Co^{2+}, Al^{3+}, Pb^{2+}, Ni^{2+} and Sr^{2+} were investigated through UV-Vis spectrophotometric method as shown in Figure 5. NSB1 showed highest absorbance at 260 nm. Presently synthesized magnetic nanoparticles are found highly selective for lead because a prominent enhancement was observed with Pb^{2+} whereas other ions were remained unaffected.

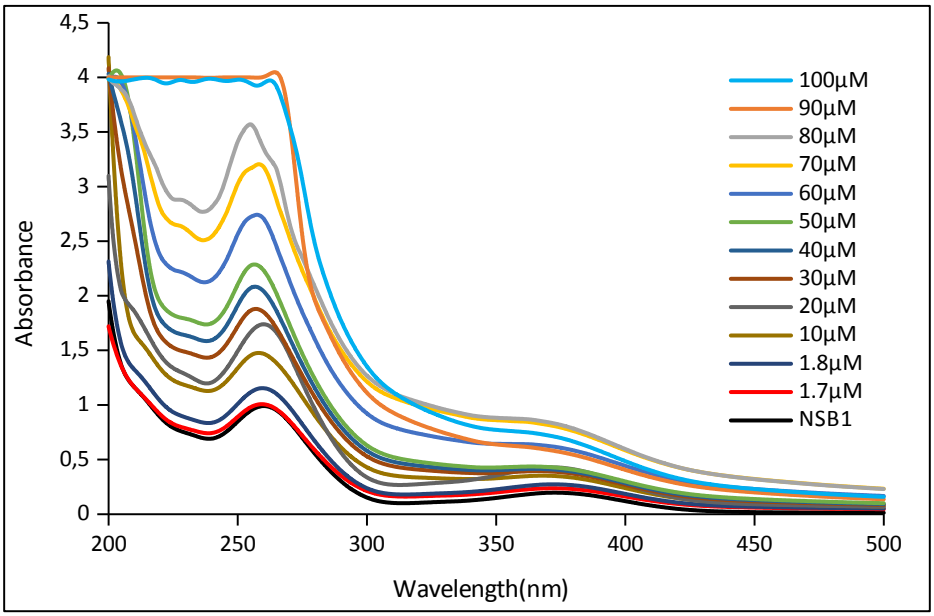

Figure 4: Screening of metals by using mixture of NSB1 and metalsalts solution (1:1).

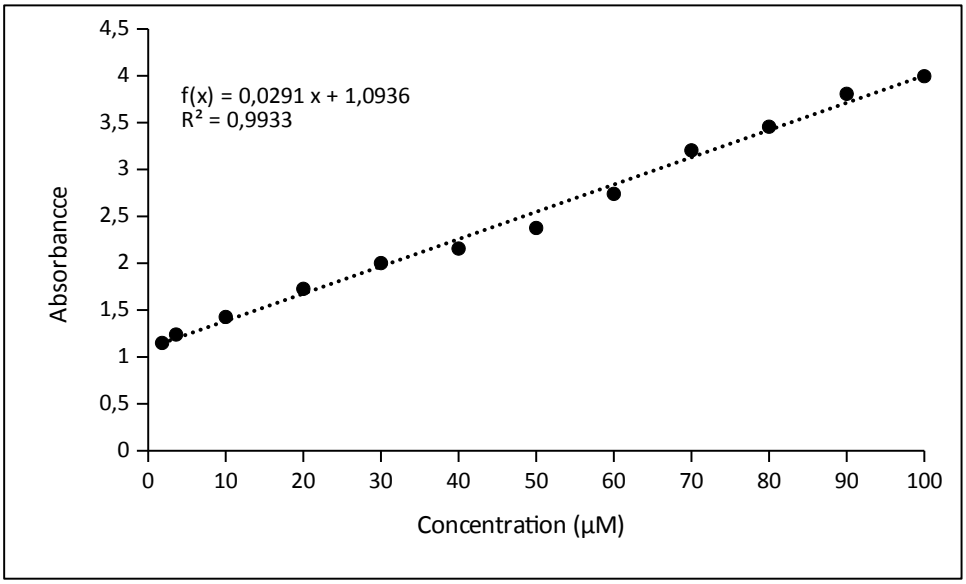

Figure 5a: Limit of detection was measured by the gradual decreasing in concentration of Pb^{2+} salt solution.

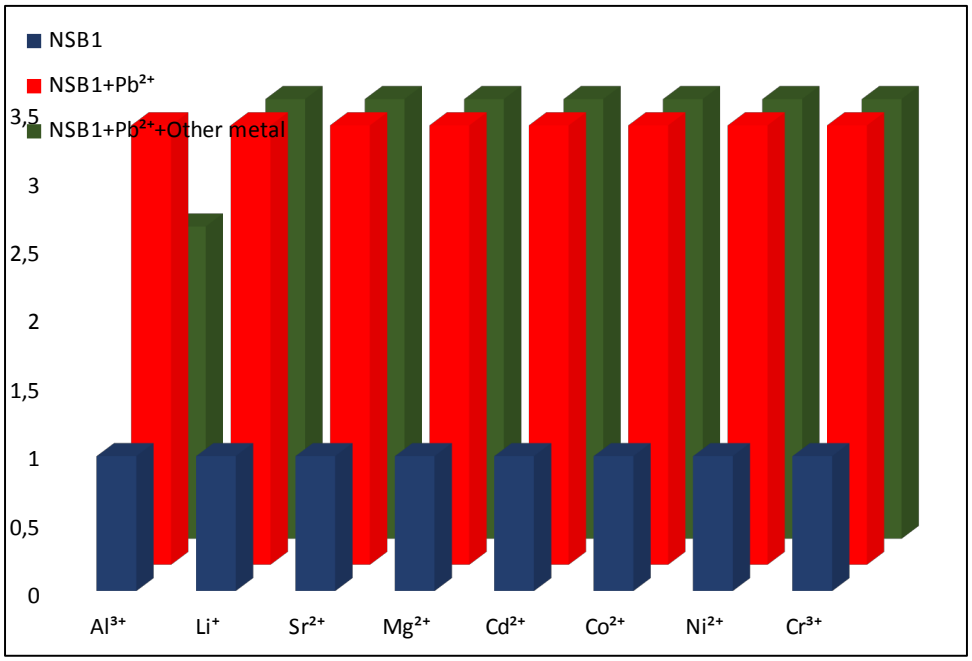

Figure 5b: Regression curve was plotted to determine uniform absorbance reduction with gradual decreasing of concentration of metal ion.

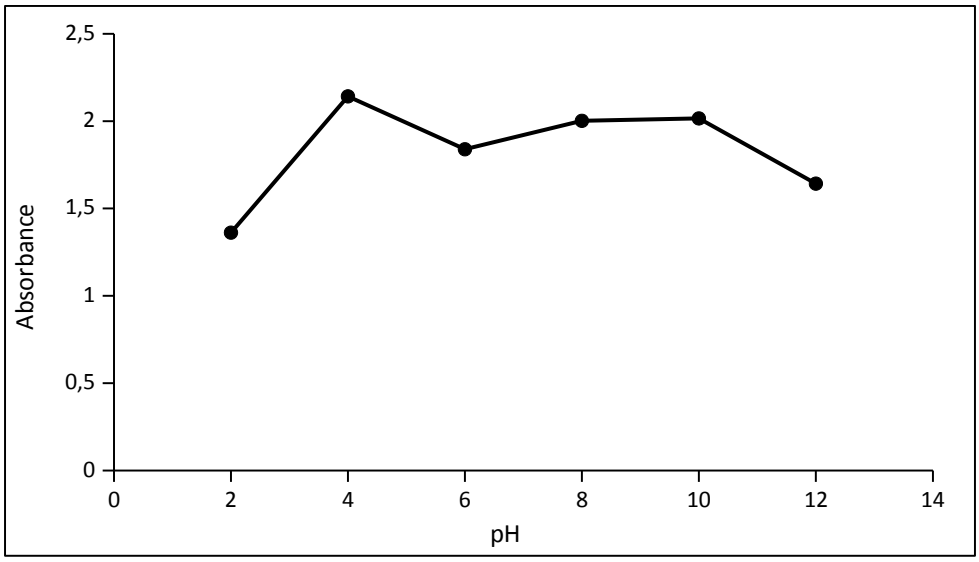

Figure 6: Competitive study of NSB1 to determine its selectivity in prevalence of other metal ions.

The binding detection limit for Pb^{2+} ions with NSB1 is shown in Figure 6a. The absorbance was recorded by successive decrease in concentration of lead while keeping the concentration of NSB1 constant. The highest selectivity for lead and NSB1 is observed in the presence of multiple metal ions (100 µM) in the recognition study as shown in Figure 7. The iron nanoparticles showed great affinity towards lead ions and this association remained undisturbed in the presence of other metal ions.

Behaviour of NSB1 towards lead ions has been evaluated at various pH (2, 4, 6, 8, 10, and 12) as presented in Figure 8. The Aqueous solutions of NaOH and HCl were used to adjust the pH values. The absorbance was decreased by addition of acid due to protonation of imine group which may destabilize nanoparticle. However the absorbance was found nearly unchanged , on increasing the pH. It may be due to the presence of free imine group which eventually stabilizes the NSB1.

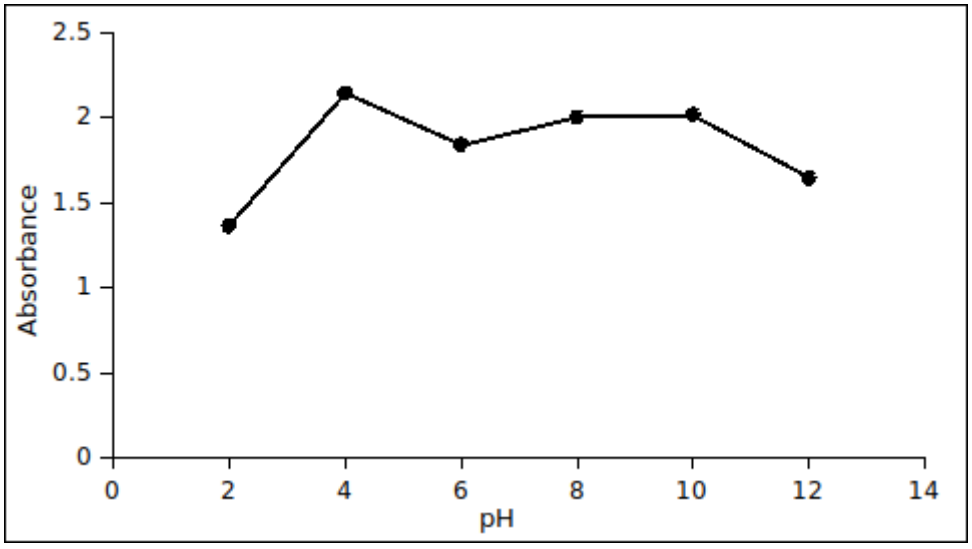

Figure 7: Binding of NSB1 with Pb^{2+} ion at different pH.

The binding ratio of complexation was measured by Job's plot in which absorbance was plotted against mole fraction of lead ions at gradual variation of mole fractions as shown in Figure 9. The favorable binding stoichiometry between NSB1 and lead ions was observed to be 1:1.

The binding constant (Ka) for NSB1 and metal complex was determined by using absorbance titration data (Figure 10). This value was computed through Benesie-Hildebrand equation (Eq. 1) and found to be 16.66×10^3 M^{-1} (30).

$$\frac{1}{A-A_0}=\frac{1}{A_1-A_0}+\frac{1}{A_1-A_0 Ka[Pb^{2+}]} \quad \text{(Eq.1)}$$

Where A_0 is the absorbance of NSB1, A is the absorbance in the presence of Pb^{2+}, A1 is the absorbance upon saturation with lead ion and Ka is the binding constant of the complex.

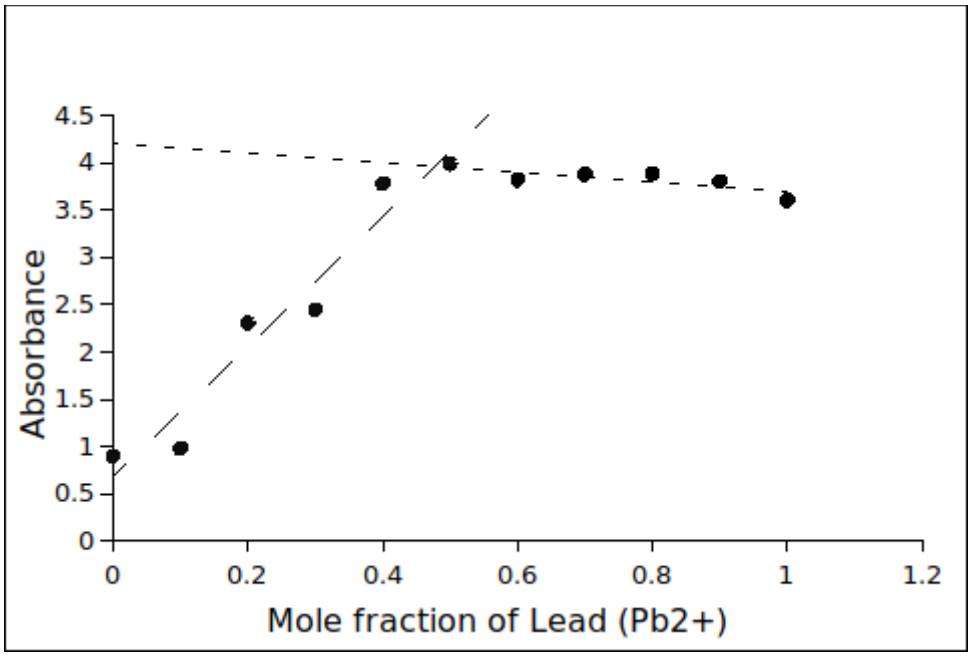

Figure 8: Job's plot of the complexation of NSB1 along with lead.

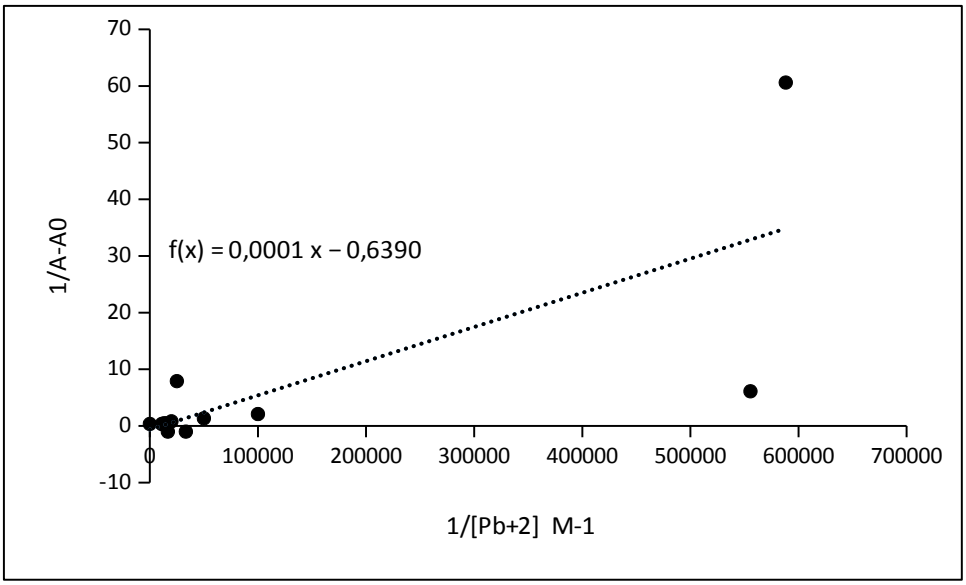

Figure 9: Stability constant of complexation measure by applying Benesi Hildebrand equation.

4. CONCLUSION

A selective magnetic nanosensor stabilized by Schiff base was prepared for rapid detection of lead ions through UV-Visible spectrophotometer. The detection of lead ions has been carried out by considering its toxic effects on environment and human. This nanosensor is cost effective very compitable to human body due to the presence of iron. The obtained nanoparticle revealed the limit of detection upto 1.7 µM for lead ions and its selectivity in the presence of other metal ions. The binding ratio and stoichiometry was found to be 1:1 as measured by Job's plot. The binding strength was also computed through Benesei-Hildebrand equation.

5. REFERENCES

1. Zhu G, Zhang C yang. Functional nucleic acid-based sensors for heavy metal ion assays. Analyst. 2014 Sep 25;139(24):6326–42. Available from: <URL>.

2. Kim HN, Ren WX, Kim JS, Yoon J. Fluorescent and colorimetric sensors for detection of lead, cadmium, and mercury ions. Chem Soc Rev. 2012;41(8):3210–44. Available from: <URL>.

3. Lin YW, Huang CC, Chang HT. Gold nanoparticle probes for the detection of mercury, lead and copper ions. Analyst. 2011;136(5):863–71. Available from: <URL>.

4. Khan H, Jamaluddin Ahmed M, Iqbal Bhanger M. A simple spectrophotometric method for the determination of trace level lead in biological samples in the presence of aqueous micellar solutions. Spectroscopy. 2006;20(5–6):285–97. Available from: <URL>.

5. Clayton GD, Clayton FE. Patty's industrial hygiene and toxicology. Vol. 2A. Toxicology. John Wiley & Sons, Inc., Baffins Lane, Chichester, Sussex PO19 1DU; 1981. ISBN: 978-0-471-16042-7.

6. Steenland K, Boffetta P. Lead and cancer in humans: Where are we now? Am J Ind Med. 2000 Sep;38(3):295–9. Available from: <URL>.

7. Aragay G, Pons J, Merkoçi A. Recent Trends in Macro-, Micro-, and Nanomaterial-Based Tools and Strategies for Heavy-Metal Detection. Chem Rev. 2011 May 11;111(5):3433–58. Available from: <URL>.

8. Rivas RE, López-García I, Hernández-Córdoba M. Microextraction based on solidification of a floating organic drop followed by electrothermal atomic absorption spectrometry for the determination of ultratraces of lead and cadmium in waters. Anal Methods. 2010;2(3):225. Available from: <URL>.

9. Grindlay G, Mora J, Gras L, de Loos-Vollebregt MTC. Ultratrace determination of Pb, Se and As in wine samples by electrothermal vaporization inductively coupled plasma mass spectrometry. Analytica Chimica Acta. 2009 Oct;652(1–2):154–60. Available from: <URL>.

10. Hsieh HF, Chang WS, Hsieh YK, Wang CF. Lead determination in whole blood by laser ablation coupled with inductively coupled plasma mass spectrometry. Talanta. 2009 Jul 15;79(2):183–8. Available from: <URL>.

11. Miao X, Ling L, Shuai X. Ultrasensitive detection of lead(ii) with DNAzyme and gold nanoparticles probes by using a dynamic light scattering technique. Chem Commun. 2011;47(14):4192. Available from: <URL>.

12. Beqa L, Singh AK, Khan SA, Senapati D, Arumugam SR, Ray PC. Gold Nanoparticle-Based Simple Colorimetric and Ultrasensitive Dynamic Light Scattering Assay for the Selective Detection of Pb(II) from Paints, Plastics, and Water Samples. ACS Appl Mater Interfaces. 2011 Mar 23;3(3):668–73. Available from: <URL>.

13. Nie D, Wu H, Zheng Q, Guo L, Ye P, Hao Y, et al. A sensitive and selective DNAzyme-based flow cytometric method for detecting Pb^{2+} ions. Chem Commun. 2012;48(8):1150–2. Available from: <URL>.

14. Wang B, Luo B, Liang M, Wang A, Wang J, Fang Y, et al. Chemical amination of graphene oxides and their

extraordinary properties in the detection of lead ions. Nanoscale. 2011;3(12):5059. Available from: <URL>.

15. Lin CH, Wu HL, Huang YL. Combining high-performance liquid chromatography with on-line microdialysis sampling for the simultaneous determination of ascorbyl glucoside, kojic acid, and niacinamide in bleaching cosmetics. Analytica Chimica Acta. 2007 Jan;581(1):102–7. Available from: <URL>.

16. Hou R, Niu X, Cui F. A label-free biosensor for selective detection of DNA and Pb $^{2+}$ based on a G-quadruplex. RSC Adv. 2016;6(10):7765–71. Available from: <URL>.

17. Zhao XH, Kong RM, Zhang XB, Meng HM, Liu WN, Tan W, et al. Graphene–DNAzyme Based Biosensor for Amplified Fluorescence "Turn-On" Detection of Pb $^{2+}$ with a High Selectivity. Anal Chem. 2011 Jul 1;83(13):5062–6. Available from: <URL>.

18. Wang X, Guo X. Ultrasensitive Pb2+ detection based on fluorescence resonance energy transfer (FRET) between quantum dots and gold nanoparticles. Analyst. 2009;134(7):1348. Available from: <URL>.

19. Hu ZQ, Lin C sheng, Wang XM, Ding L, Cui CL, Liu SF, et al. Highly sensitive and selective turn-on fluorescent chemosensor for Pb2+ and Hg2+ based on a rhodamine–phenylurea conjugate. Chem Commun. 2010;46(21):3765. Available from: <URL>.

20. Li T, Dong S, Wang E. A Lead(II)-Driven DNA Molecular Device for Turn-On Fluorescence Detection of Lead(II) Ion with High Selectivity and Sensitivity. J Am Chem Soc. 2010 Sep 29;132(38):13156–7. Available from: <URL>.

21. Wu J, Qin Y. Polymeric optodes based on upconverting nanorods for fluorescence measurements of Pb2+ in complex samples. Sensors and Actuators B: Chemical. 2014 Mar;192:51–5. Available from: <URL>.

22. Tümay SO, Şanko V, Şenocak A, Demirbas E. A hybrid nanosensor based on novel fluorescent iron oxide nanoparticles for highly selective determination of Hg $^{2+}$ ions in environmental samples. New J Chem. 2021;45(32):14495–507. Available from: <URL>.

23. Ge L, Liu H. Engineering Grey Nanosystem as Activatable Ratio-colorimetric Probe for Detection of Lead Ions in Preserved Egg. ANAL SCI. 2020 Nov;36(11):1407–13. Available from: <URL>.

24. Elbaz J, Shlyahovsky B, Willner I. A DNAzyme cascade for the amplified detection of Pb2+ ions or l-histidine. Chem Commun. 2008;(13):1569. Available from: <URL>.

25. Liu XH, Zheng H, Zhong L, Huang S, Karki K, Zhang LQ, et al. Anisotropic Swelling and Fracture of Silicon Nanowires during Lithiation. Nano Lett. 2011 Aug 10;11(8):3312–8. Available from: <URL>.

26. Reese CE, Asher SA. Photonic Crystal Optrode Sensor for Detection of Pb $^{2+}$ in High Ionic Strength Environments. Anal Chem. 2003 Aug 1;75(15):3915–8. Available from: <URL>.

27. Hamid A, Aamer S, Farukh J, Abdul B, Irfan ZQ, Abdul A, et al. Synthesis, Characterization, Biological and Docking Simulations of 4-(Benzylideneamino) Benzoic Acids ((1)). CHINESE JOURNAL OF STRUCTURAL CHEMISTRY. 2021;40(3):291–300.

28. Valarmathy G, Subbalakshmi R, Sabarika B, Nisha C. Schiff bases derived from 4-amino-N-substituted benzenesulfonamide: synthesis, spectral characterisation and MIC evaluation. Bull Chem Soc Eth. 2021 Oct 24;35(2):435–48. Available from: <URL>.

29. Ferroudj N, Nzimoto J, Davidson A, Talbot D, Briot E, Dupuis V, et al. Maghemite nanoparticles and maghemite/silica nanocomposite microspheres as magnetic Fenton catalysts for the removal of water pollutants. Applied Catalysis B: Environmental. 2013 Jun;136–137:9–18. Available from: <URL>.

30. Shah K, Hassan E, Ahmed F, Anis I, Rabnawaz M, Shah MR. Novel fluorene-based supramolecular sensor for selective detection of amoxicillin in water and blood. Ecotoxicology and Environmental Safety. 2017 Jul;141:25–9. Available from: <URL>.